Available online at www.sciencedirect.com
ScienceDirect
International Journal of Heat and Fluid Flow 28 (2007) 1073–1091
International Journal of HEAT AND FLUID FLOW
www.elsevier.com/locate/ijhff

Turbulence modeling for flows around convex features giving rapid eddy distortion

P.G. Tucker [a,*], Y. Liu [b]

[a] The Whittle Laboratory, Department of Engineering, University of Cambridge, Madingly Road, Cambridge CB3 0DY, UK
[b] School of Naval Architecture Engineering, Dalian University of Technology, Dalian 116024, China

Received 17 January 2006; received in revised form 27 March 2007; accepted 10 April 2007
Available online 18 June 2007

Abstract

Reynolds averaged Navier–Stokes model performances in the stagnation and wake regions for turbulent flows with relatively large Lagrangian length scales (generally larger than the scale of geometrical features) approaching small cylinders (both square and circular) is explored. The effective cylinder (or wire) diameter based Reynolds number, $Re_W \leqslant 2.5 \times 10^3$. The following turbulence models are considered: a mixing-length; standard Spalart and Allmaras (SA) and streamline curvature (and rotation) corrected SA (SARC); Secundov's v_t-92; Secundov et al.'s two equation v_t–L; Wolfshtein's k–l model; the Explicit Algebraic Stress Model (EASM) of Abid et al.; the cubic model of Craft et al.; various linear k–ε models including those with wall distance based damping functions; Menter SST, k–ω and Spalding's LVEL model. The use of differential equation distance functions (Poisson and Hamilton–Jacobi equation based) for palliative turbulence modeling purposes is explored. The performance of SA with these distance functions is also considered in the sharp convex geometry region of an airfoil trailing edge.

For the cylinder, with $Re_W \approx 2.5 \times 10^3$ the mixing length and k–l models give strong turbulence production in the wake region. However, in agreement with eddy viscosity estimates, the LVEL and Secundov v_t-92 models show relatively little cylinder influence on turbulence. On the other hand, two equation models (as does the one equation SA) suggest the cylinder gives a strong turbulence deficit in the wake region. Also, for SA, an order or magnitude cylinder diameter decrease from $Re_W = 2500$ to 250 surprisingly strengthens the cylinder's disruptive influence. Importantly, results for $Re_W \ll 250$ are virtually identical to those for $Re_W = 250$ i.e. no matter how small the cylinder/wire its influence does not, as it should, vanish. Similar tests for the Launder–Sharma k–ε, Menter SST and k–ω show, in accordance with physical reality, the cylinder's influence diminishing albeit slowly with size. Results suggest distance functions palliate the SA model's erroneous trait and improve its predictive performance in wire wake regions. Also, results suggest that, along the stagnation line, such functions improve the SA, mixing length, k–l and LVEL results. For the airfoil, with SA, the larger Poisson distance function increases the wake region turbulence levels by just under 5%.

Keywords: Rapid distortion; Stagnation; Wake flows; RANS; Flow over cylinder

1. Introduction

In gas turbines, as well as high free stream turbulence intensities, the Lagrangian eddies of scale, L_0, approaching turbine blades are of significant size relative to the blade leading edge effective diameter, D ($L_0/D \approx 2$). As shown by Wang et al. (1998) and Maslov et al. (1999), in the leading stagnation region, this presents some important turbulence modeling challenges. Also, for fin pin heat sinks such as found in, for example, electronic systems, the peripheral fins can encounter large eddies relative to their size. Tall buildings and chimneys (see Hunt, 1976) can also experience impingement from eddies of significant relative scale.

On the other hand the performances of turbulence models around and downstream of sharp convex features (i.e. blade trailing edges, vortex generators and also features like chevrons – serrations – at aero engine jet outlets) is

* Corresponding author. Tel.: +44 1223 332600; fax: +44 1223 332662.
E-mail address: Pg23@cam.ac.uk (P.G. Tucker).

0142-727X/$ - see front matter © 2007 Elsevier Inc. All rights reserved.
doi:10.1016/j.ijheatfluidflow.2007.04.020

an important area of engineering interest. Models can exhibit complex behavior in such regions (see Tucker et al., 2005). For example, with multi-element airfoils differences in upstream turbulence conditions can give rise to non-unique solutions. Also, with hybrid LES/RANS (Large Eddy Simulation/Reynolds Averaged Navier–Stokes) and jets there is the potential for excessive convected eddy viscosity levels, generated from RANS zones around chevrons, to laminarize resolved scales.

A useful prototype for studying both these essentially leading and trailing edge influences is the flow over a thin cylinder of diameter D in a channel of height H. The channel height will define the Lagrangian scales approaching the cylinder. At the leading edge, depending on L/D, the oncoming turbulence can be either strongly influenced by streamline curvature or stagnation. Downstream, the relevant Reynolds number is $Re_W = \rho U_0 D/\mu$ where U_0 is the fluid approach velocity, D the cylinder's diameter, μ the fluid's dynamic viscosity and ρ its density. In this region, there is a potential complex interaction between the free stream and wake turbulence. Although little is known about the flow physics of this latter interaction (see Hinze, 1975) it is worth noting some of the available information.

1.1. Flow physics

Through differentiation of a Gaussian fit to measured mean wake velocity profiles and drag considerations Hinze (1975) derives the following semi-analytical expression for cylinder wake turbulent viscosity levels around the channel centre line

$$\mu_{t,w} = 0.0164\rho U_0 D \tag{1}$$

where U_0 and D are as defined above. Similarly, Hussain and Reynolds (1975) normalize measured turbulent shear stresses by differentiated velocities (i.e. evaluate centre line turbulent viscosities $\mu_{t,c}$ as equal to $-\rho\overline{u'v'}/(\mu \mathrm{d}U/\mathrm{d}y)$) to gain the following expression for turbulent viscosity around a channel centre line

$$\mu_{t,c} = 0.07\rho u_\tau \delta \tag{2}$$

In the above u_τ is the friction velocity and δ the boundary layer thickness. Here, in Eq. (2) the factor of 10 error in the Hussain and Reynolds (1975) paper has been corrected. It is worth noting that, since $\partial U/\partial y$ tends to zero at the channel centre line the above expression will have some uncertainty. Hence, it is easiest to understand as an equation that applies in the vicinity of the centre line (where $\mu_{t,c}$ varies slowly) and not exactly on it.

Here, mostly a cylinder in a channel, of height H, which has $D = H/40$ and $Re_W \approx 2.5 \times 10^3$ is studied. For this, Eqs. (1) and (2) give $\mu_{t,w}/\mu_{t,c} \approx 0.5$. Hence, the wake turbulence is expected to be lower than the ambient (that occurring in a channel with no cylinder). Although little is understood of the way external turbulence interacts with wakes it is clear that external turbulence can trigger the early transition of boundary layers on the upstream side of bluff bodies. As would be expected, this in turn reduces wake drag. The cylinder's wake will be buffeted by turbulence. This will increase turbulence levels/mixing (see Britter et al., 1979) and probably widen the wake which has a Gaussian velocity distribution in the time mean. Hence, following the eddy viscosity evaluation procedure of Hinze (1975), $\mu_{t,w}$ will increase towards the surrounding elevated $\mu_{t,c}$ level. The above discussion is probably pertinent to most bluff bodies of scale D placed in external turbulence. This suggestion is enforced by the work of Britter et al. (1979) where agreement is found between theoretical analysis (see Hunt, 1973) and measurements for a range of bluff bodies. Hence, under the conditions considered here, it is expected that analysis of the data for non-circular geometries has relevance, with errors/variations of geometrical form being insignificant.

The interaction of the upstream ambient turbulence on the stagnation region just upstream of cylinders was theoretically analyzed by Hunt (1973) using the 'rapid distortion' theory simplification. With this, the eddy life time $L/\sqrt{2k_0/3}$ (k_0 is magnitude of the upstream turbulence kinetic energy) is considered large compared with the mean flow time scale centered on the cylinder – D/U_0. This implies the following ratio:

$$\psi = \frac{\sqrt{2k_0/3}}{U_0}\frac{D}{L} \ll 1 \tag{3}$$

Hence the turbulence is assumed to be subjected to such a rapid distortion that it is modified by the mean flow but not (non-linear) self interactions between different turbulent scales. Hunt (1973) explored the limiting states of $D/L_0 \to \infty$ and $D/L_0 \to 0$. The theoretical analysis of Hunt suggests that for $D/L_0 \to \infty$ streamline curvature, in the mean flow, strains approaching eddies giving rise to upstream normal Reynolds stress generation. Conversely, for $D/L_0 \to 0$ the normal Reynolds stress near the cylinder is damped by the blocking effect of the cylinder. In the stagnation region, the normal Reynolds stress greatly controls heat transfer. Hence, Wang et al. (1998) find for large L_0 (and a high free stream turbulence intensity) apparently suppressed heat transfer. This is consistent with the heat transfer correlation of Dullenkopf and Mayle (1995) which (importantly) includes the influence of L_0. Hunt's work implies that for distances x of about 2 or $3L_0$ upstream from the cylinder free stream turbulence conditions prevail. Closer to the cylinder, but outside the upstream cylinder boundary layer ($x \gg \delta$, where $\delta \propto 1/Re^{1/2}$) the turbulence characteristics are a function of both D/L_0 and x/L_0. Hence, in this region conditions are not a function of upstream turbulence intensity but L_0. As discussed later, this region presents a key turbulence modeling challenge. For $x < \delta$ (where x and δ are now focused on the cylinder) turbulence conditions become a function of $D/L_0, x/L_0$ and Reynolds number. Hence, in summary, from the above, for $Re_W \approx 2.5 \times 10^3$ we might well expect that with respect to the region downstream of the cylinder, the cylinder has a

relatively passive role. Ideally RANS models should reflect this, predicting no great $\mu_{t,c}$ disruption. Around the upstream stagnation region the cylinder should cause significant normal stress damping.

1.2. Expected turbulence model traits

Having discussed what is expected to happen and the broad flow physics, the key question is how will RANS models deal with the situation of a small cylinder placed in a turbulent ambient flow where the energy containing eddies approaching the cylinder, are of size L_0 which is greater than the cylinder size ($L_0/D > 1$)? It is expected that with most turbulence models the cylinder proximity will activate turbulence damping terms perhaps via use of the normal wall distance d. On the other hand, extra fluid straining caused by the cylinder's presence, will generate turbulence. The balance of these processes, which is to an extent considered in Britter et al., will govern the ultimate μ_t levels around the cylinder. It seems likely that, in accordance with physical expectations, if the channel ambient $\mu_{t,c}$ is higher than the wake $\mu_{t,w}$ diffusion modeling terms, available in many turbulence models (those with at least one transport equation), will allow the prediction of an elevated $\mu_{t,w}$. Now turning attention more specifically to the stagnation zone, it should be noted that RANS models are invalid for $L_0 \gg \delta$ (see Secundov et al., 2001). Also, as noted above, for $3L_0 > x \gg \delta$ (where δ relates to the cylinder boundary layer), experiments suggest there is no free stream turbulence intensity dependence but a strong dependence on the convection of L_0. However, simpler one and zero equation models have no means of modeling L_0 convection. Also, transport equations for turbulence energy used in many RANS models are unlikely to sufficiently decrease (relative to L_0) the convection of turbulence energy/intensity from upstream into the zone which should be unaffected by this quantity. Hence they are likely to yield results with an excessive dependency on upstream turbulence conditions. This would, in part, explain why two equation models dramatically over predict stagnation region heat transfer (see Ashforth-Frost and Jambunathan, 1996, where, with a high Reynolds number k–ε model, the stagnation region heat transfer is over predicted by 300%) and turbulence levels (see Franke and Rodi, 1993). The term $\overline{u_i'u_j'}\partial U_i/\partial x_j$ used in the k–ε (and k–l) model is an exact representation of turbulence energy production. However, except for simple shear flows, the $\overline{u_i'u_j'}$ terms are not well modeled through strain rate (S_{ij}). Indeed, in the stagnation region, S_{ij} can become high, giving a further reason for the over prediction of turbulence and hence heat transfer. A partial remedy is the *ad hoc* stagnation region modification given by Kato and Launder (1993). This essentially involves vorticity in the production term. In stagnation regions, where the flow becomes close to irrotational, vorticity tends to zero hence reducing energy production. It is worth noting here that SA (see Spalart and Allmaras, 1994) also uses vorticity in the production term but for simple shear flows vorticity and strain rate become identical. For the SARC (streamline curvature – and rotation – corrected SA, see Spalart and Shur, 1997) model, the SA standard production term is premultiplied by a function involving strain rate normalized by vorticity. Since all the two equation models, used here, make use of strain rate in production terms it is expected that these models will over-predict turbulence in the stagnation region.

Many popular industrial RANS models use d for turbulence destruction modeling. Hence, it seems important to discuss the physical connotations of this variable in relation to the current prototype problem.

1.3. Role of normal wall distance

For the following discussion the curved surface schematics in Fig. 1 are helpful. Frame (a) is for a mildly convex/concave geometry and (b) a more heavily convex/concave geometry. If one considers the two points located at d_1 and d_2 either side of the curved surfaces shown in Fig. 1 it is understandable that the more enclosed left hand field points (represented by d_1) will experience more turbulence damping (due to the blocking influence of the wall on fluctuations normal to it and the viscous damping of wall parallel components) than the right (it is especially so for Frame (b)). This is consistent with the DNS (Direct Numerical Simulation) observations of Mompean et al. (1996) for flow in a convex 90° corner. Modification of d to some $\tilde{d}$ can be a convenient means of appropriately sensitizing turbulence models to small cylindrical convex and concave features (see Tucker et al., 2005; Tucker, 2003). Consistent with the above ideas Launder et al., 1975 proposed that a preferable distance-function ($\tilde{d}$) behavior is perhaps best captured in terms of the elemental *solid* angle, $d\omega$. This is the solid angle subtended by a patch, on say a surface of radius of curvature $D/2$, a distance d from a field point. Hence Launder et al. proposed

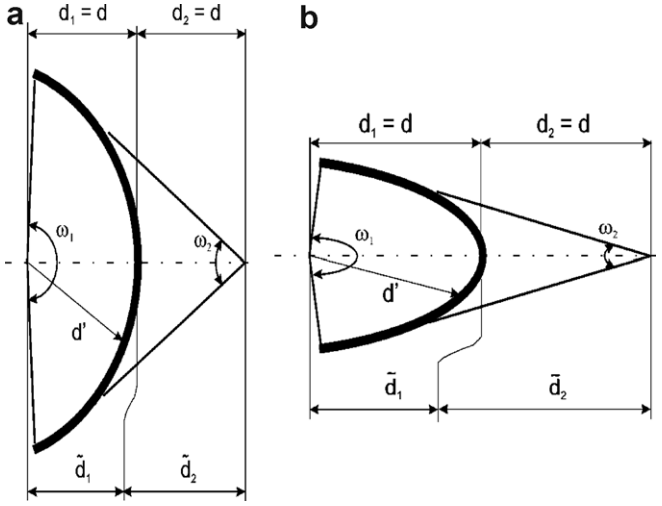

Fig. 1. Schematic showing nature of solid angle based wall distance equation of Launder et al.: (a) mildly convex/concave geometry and (b) more heavily convex/concave geometry.

$$\frac{1}{\tilde{d}} = \frac{1}{\pi}\int \frac{d\omega}{d'} \tag{4}$$

(here we correct the factor of 2 error in the equation of Launder et al.) where d' is a continuous wall distance with no restriction on surface normality. In a convex geometry region, Eq. (4) will give $\tilde{d} > d$ and in a concave region $\tilde{d} < d$. Hence, Fig. 1 suggests the nature of and inspiration for the solid angle based wall distance equation of Launder et al. As can be seen, in both frames $\tilde{d}_1 < \tilde{d}_2$, however where the solid angle is smaller the disparity increases. It should be noted that solid angles are a three-dimensional concept. However, to make Fig. 1 easier to visualize usual angles have been considered.

Inline with the above accuracy, or physics, considerations (Spalding, 1994) proposed the LVEL turbulence model. A key element of this is a Poisson differential equation for the wall distance related function ϕ. This equation is given below.

$$\nabla^2\phi = -1 \tag{5}$$

The variable ϕ can be converted into a wall distance function through the auxiliary equation below:

$$\tilde{d} = \pm\sqrt{\sum\nolimits_{j=1,3}\left(\frac{\partial\phi}{\partial x_j}\right)^2} + \sqrt{\sum\nolimits_{j=1,3}\left(\frac{\partial\phi}{\partial x_j}\right)^2 + 2\phi} \tag{6}$$

The derivation of (6) includes the assumption that surfaces are extensive in the non wall normal directions. Eqs. (5) and (6) have all the desirable traits of Eq. (4), noted above i.e. for a single flat surface $\tilde{d} = d$, in a convex geometry region $\tilde{d} > d$ and in a concave region $\tilde{d} < d$.

Fares and Schroder (2002) also derived a differential equation for $\tilde{d}$ which again is aimed at reflecting the traits of Eq. (4). An exact equation for d that can be readily derived using simple coordinate geometry is the hyperbolic Eikonal equation below

$$|\nabla\phi| = 1 + \Gamma\nabla^2\phi \tag{7}$$

where $\Gamma \to 0$ giving viscosity solutions. However, if $\Gamma = f(\phi)$ the resulting Hamilton–Jacobi (HJ) equation will also give the traits of Eqs. (4)–(6) above (see Tucker et al., 2005). Tucker (2003), motivated by dimensional homogeneity and the need that as $d \to 0, \tilde{d} = d$ but $\nabla^2\phi \to \infty$ suggests

$$\Gamma = \tilde{\varepsilon}\phi \tag{8}$$

where $\tilde{\varepsilon}$ is a constant.

Partly in accordance with Spalding's line of thought that the wall distance function $\tilde{d}$ should be part of a turbulence model Spalart (1992) developed his own $\tilde{d}$ model to go in what is described as the POEM model. Essentially, the $\tilde{d}$ for this model came from a modified version of Eq. (4). Importantly, as shown in Tucker (2003), Tucker et al. (2005) and Sethian (1999), Eqs. (5)–(7) can, relative to search procedures, be rapidly solved.

In the current paper, first RANS model traits, especially in relation to different $\tilde{d}$ distributions, when predicting the flow over small cylinders are considered. The initial focus is the wake region followed then by consideration of the stagnation zone. Finally, the trailing edge region of a NACA4412 airfoil and the influence of $\tilde{d}$ on turbulence in this zone is explored. The turbulence modeling issues associated with the airfoil sharp convex trailing edge are considered to be in many ways akin to those for the downstream side of a small cylinder. The following RANS models are considered:

Standard mixing-length with Van Driest's damping function (ML);
SA;
SARC;
Secundov's v_t-92 (see Secundov et al., 2001);
Secundov et al.'s two equation v_t–L (see Secundov et al., 2001);
Wolfshtein's (1969) k–l model;
the Explicit Algebraic Stress Model (EASM) of Abid et al. (1996);
original EASM with Abe et al. (1994) (AKN) damping functions;
the cubic model of Craft et al. (1996);
the linear Launder and Sharma (1974) (LS), Chien (1982) and AKN k–ε models;
Wilcox's (1988) and Wilcox's (2004) k–ω models;
Menter SST (see Menter, 1993) (with and without shear stress transport terms) and
Spalding's (1994) LVEL model.

The Yap (1987) and Kato and Launder (1993) correction terms are also considered.

2. Numerical methods and models

2.1. Numerical solution approaches

For the cylinder flow, to allow a wider range of turbulence models to be more easily considered essentially two different computer programs are used. These are the NTS (Shur et al. (2003)) and NEAT (see Tucker (2001)) programs. Fig. 2 shows the different grids used in these. NTS is an overset grid code. The solution grid used in this program is shown in Fig. 2a and c. Frame c is a zoomed in view at the cylindrical surface. The 'O' grid, used to map the cylindrical surface, has just over 8000 nodes and the outer Cartesian grid 33,604 nodes. However, most simulations are run with also doubling of this number of grid cells. Also, for smaller Re_W and two equation models which have higher grid demands a quadrupling of the number of nodes is used. Hence, for these simulation nearly 50 layers of grid nodes are committed to just the viscous sublayer of the cylinders.

NEAT is used in two modes. With one, the cells around the cylinder are treated in a numerically identical fashion to the trimmed cell approach described in Tucker and Pan (2000). As shown in Pan and Tucker (2001) the approach

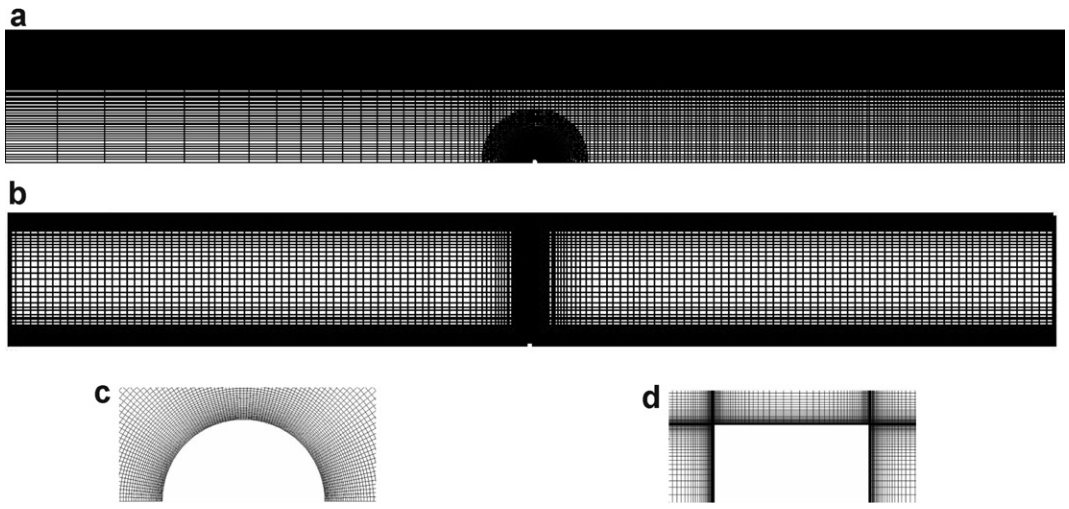

Fig. 2. Solution grids: (a) NTS code, (b) NEAT code, (c) NTS near circular cylinder and NEAT near square cylinder.

works well for flows over cylinders. Also, *NEAT* is used with a square cylinder placed at the channel centre having an equivalent scale to the circular cylinder. This mesh, shown in Fig. 2b and d, has over 45,000 cells in the half channel. The trimmed cell mesh is around 1/3rd the density of the one for the square cylinder. However, the results are surprisingly similar, confirming that the finer meshes used here for all quantitative results are adequate at illustrating the points to be made. As can be seen from Fig. 2b, with the mono-block NEAT code, to resolve the cylinder, a fine mesh around the channel centre lines is required.

For NTS, 3rd order upwinding is used in the convective terms. For NEAT the hybrid scheme (see Spalding, 1972) is implemented. Both these schemes will assist with suppressing any wake unsteadiness.

Solution methods for the Poisson and Hamilton–Jacobi distance function equations are given in Tucker (2003) and Tucker et al. (2005) and so are also not repeated here.

2.2. Turbulence models

Along with the program in which they are implemented and the nature of damping functions, the turbulence models tested are summarized in Table 1. Both the 1988 and 2004 versions of the k–ω model are tested. The latter is intended to deal with the excessive free stream dependence of the original model. Most of the models used are well known and comprehensively documented in the references given at the end of the introduction. Hence, since such a wide range of models are considered, to save space, only model traits felt most pertinent to the current work are discussed in this section. However, for the less well known v_t-92, $v_t - L$ (where many publications are in Russian), LVEL and also SARC models fuller descriptions are included in the Appendix.

The damping in the tabulated models is generally facilitated through the following Reynolds number formulations:

Table 1
Summary of RANS models, the basis of their damping functions and programs these models are implemented in

Model	Uses d?	Code	Damping basis	No. of equations
Van Driest damping function based mixing length model (ML)	Yes	NEAT	y^+	0
LVEL model of Spalding	Yes	NEAT	y^+	0
Wolfshtein k–l	Yes	NEAT/NTS	y^*	1
Spalart and Allmaras (SA)	Yes	NEAT/NTS	–	1
SARC	Yes	NTS	-	1
Secundov v_t-92	Yes	NTS	–	1
v_t–L	Yes	NTS	–	2
Launder-Sharma (LS) k–ε	No	NEAT/NTS	Re_T	2
Chien k–ε	Yes	NEAT	y^+, Re_T	2
AKN k–ε	Yes	NEAT	y^*, Re_T	2
Abid et al. EASM	Yes	NEAT	y^+, Re_y	2
AKN EASM	Yes	NEAT	y^*, Re_T	2
Wilcox k–ω (1988 and 2004 versions)	No	NTS	–	2
Menter SST (also minus SST terms)	Yes	NTS	–	2
Cubic model of Craft et al.	No	NEAT	Re_T	2

$$Re_T = \frac{\rho k^2}{\varepsilon\mu}, \quad Re_y = \frac{\rho k^{1/2} d}{\mu}, \quad y^* = \frac{0.55\rho k^{1/2} d}{\mu},$$
$$y^+ = \frac{\rho u_\tau d}{\mu} \tag{9}$$

As can be seen, the last three listed above involve d. Along different lines (allowing the blocking effect of the wall to be felt through pressure signals) SA and v_t-92 have destruction ($\widehat{D}$) terms of the following type

$$\widehat{D} = -C_1 \mu_t^2 \frac{1}{d^2} \tag{10}$$

With SA, $\widehat{D}$ is further multiplied by a near wall non-viscous destruction element/function f_w which increases towards walls. Because the turbulence destruction term (Eq. (10)) decays too slowly in the outer part of the boundary layer, hence giving inaccurate boundary layer skin friction values, this term is necessary. It has the following form:

$$f_w \propto \frac{1}{d^2} + C_2\left(\frac{1}{d^{12}} - \frac{1}{d^2}\right)\left(\frac{1 + C_3}{\left(\frac{1}{d^2} + C_2\left(\frac{1}{d^{12}} - \frac{1}{d^2}\right)\right)^6 + C_3^6}\right)^{1/6} \tag{11}$$

As can be seen this function is fairly tortuous in d. The f_w function is a major element that distinguishes the SA model from Secundov's models (see Spalart and Allmaras, 1994).

Also, near walls essentially (note in the log layer $\mu_t = \rho\kappa d u_\tau$)

$$\mu_t = \rho\kappa d u_\tau f_{v1} \tag{12}$$

where the viscous 'damping function'

$$f_{v1} = \frac{1}{1 + \left(\frac{C_4}{\kappa y^+}\right)^3} \tag{13}$$

The production term also needs a modifying function and this is as follows:

$$f_{v2} = 1 - \frac{1}{\frac{1}{\kappa y^+} + f_{v1}} \tag{14}$$

Note, unlike the two equation models, SA and v_t-92 do not contain any L_0 information. The v_t–L extends v_t-92 by including a transport equation for L. This allows the influence of free stream eddies approaching an object to be modeled. The transport equation has the usual convection and diffusion terms. A key L destruction term ($\widehat{D}_L$) is proportional to

$$\widetilde{D}_L \propto \frac{\mu_t}{\rho}\frac{L}{d^2} \tag{15}$$

This describes the decrease in L due to wall proximity. An important scaling factor of terms in the differential equation for L is

$$\Phi \propto \frac{\rho L^2}{\mu_t}\frac{\partial L}{\partial x_i} S_{ik} \frac{\partial L}{\partial x_k} \tag{16}$$

where the strain rate is defined as follows $S_{ik} = 0.5(\partial U_i/\partial x_k + \partial U_k/\partial x_i)$. This phenomenological term becomes maximum in stagnation regions and tends to zero in simple shear flows.

It is important to note that the LVEL model differentiates a Taylor series based single equation fit to the 'law of the wall.' This differentiation yields a dimensionless eddy viscosity. The model is intended to be robust in the sense of giving physically plausible results on extremely coarse grids, where velocity gradients cannot be resolved accurately. This latter aspect is important for more elaborate turbulence models containing numerous gradient terms.

The influence of the Yap (1987) correction (a source term extension in the ε equation to prevent excessive turbulence production) is also considered. As noted in the introduction, a partial remedy to the excessive stagnation region turbulence kinetic energy found with the k–ε model is the modification given by Kato and Launder (1993). With this, in the stagnation region, the production is re-expressed as

$$\overline{u_i' u_j'}\frac{\partial U_i}{\partial x_j} = \frac{\mu_t}{\rho} S\Omega \tag{17}$$

where S and Ω are strain and vorticity related parameters

$$S = \sqrt{\frac{1}{2}\left(\frac{\partial\langle U_i\rangle}{\partial x_j} + \frac{\partial\langle U_j\rangle}{\partial x_i}\right)^2};$$
$$\Omega = \sqrt{\frac{1}{2}\left(\frac{\partial\langle U_i\rangle}{\partial x_j} - \frac{\partial\langle U_j\rangle}{\partial x_i}\right)^2} \tag{18}$$

Because in stagnation regions, the flow is very nearly irrotational, i.e. $\Omega \approx 0$, Eq. (17) leads to a reduction in turbulence generation. For simple shear flows, the equation gives the original production term.

For the inner half of the boundary layer Menter SST uses the k–ω model. Outside this zone (to remove the free stream condition dependency of the k–ω model) the k–ε model is used in a k–ω form. The two models are blended using an expression of the form

$$\phi = F_1\phi_1 + (1 - F_1)\phi_2 \tag{19}$$

where F_1 is a hyperbolic tangent based function involving $1/d^2$ terms. The additional shear stress transport terms (SST) in the Menter model are intended to add a form of Reynolds stress transport modeling (reminiscent of Reynolds stress models) to the primary shear stress. This additional element, expressed below, (where $\tau = -\rho\overline{u'v'}$)

$$\frac{D\tau}{Dt} = \frac{\partial\tau}{\partial t} + u_k\frac{\partial\tau}{\partial x_k} \tag{20}$$

is intended for adverse pressure gradient flows. The additional transport equation means that the predicted shear stress no longer responds instantaneously to changes in the strain field. For the current case the influence of the SST element might be expected to be most significant in the wake region where the cylinder introduces a local adverse pressure gradient. Activation of the SST component

is again controlled by a hyperbolic tangent function involving a $1/d^2$ term. The Menter SST model is also considered both with and without the SST terms.

It is worth noting, as pointed out earlier, that in their standard forms all the two equation models, along with the k–l, use strain rate in the production terms. The SA model uses vorticity. For all models, unless otherwise stated, standard constants are used. A full range of validation tests for the NEAT RANS models can be found in Liu (2004).

2.3. Boundary conditions and related information

At inflow boundaries fully developed velocity profiles are specified. Also, turbulence properties are specified based on fully developed profiles generated from simulations with no cylinder. At solid walls the usual no-slip and impermeability conditions are applied. With NEAT, simulations are made to test the sensitivity of results to the assumption of centre line symmetry. Insignificant differences (in the context of the current results) are found between results where symmetry is forced and wake asymmetries allowed to develop.

It is worth noting that the dissipative k–ε model generally suppresses wake turbulence. Also, the NEAT and NTS codes share the LS, k-l and SA turbulence models. Despite one code modeling a circular cylinder and the other a square the LS, k-l and SA centre line eddy viscosity distributions are pleasingly close. Hence, in the results discussion no distinction is drawn regarding which code is used to provide the results. However, if desired this can generally be delineated from Table 1. Also, for all quantative NEAT comparisons just results for the square cylinder are presented.

For the NACA4412 case a 25,000 cell 'C' grid provides sensibly grid independent solutions. The grid extends around 20 chords downstream of the airfoil and 15 in the remaining directions. Numerical details (based on the NASA CPL30 program) can be found in Tucker et al. (2005). To save space, these will not be reproduced here.

3. Discussion of results

3.1. Cylinder results for wake region

Fig. 3 shows the ratio of eddy to mean flow time scales (ψ) as defined by Eq. (3) for the LS k–ε model and $Re_W = 2500$. As would be expected, we are around the rapid distortion turbulence regime. Hence, upstream of the cylinder $\psi \to 0$. In the wake region, we might expect eddies of scale $L \approx D$ to dominate and the k–ε model seems to correctly imply this with $\psi \approx 1$. Further aspects relating to rapid distortion, for even smaller Re_W and hence ψ, will be noted later.

Fig. 4 gives turbulent viscosity contours for $Re_W = 2.5 \times 10^3$ and the following RANS models: ML (Frame (a)); LVEL (Frame (b)); k–l (Frame (c)); SA

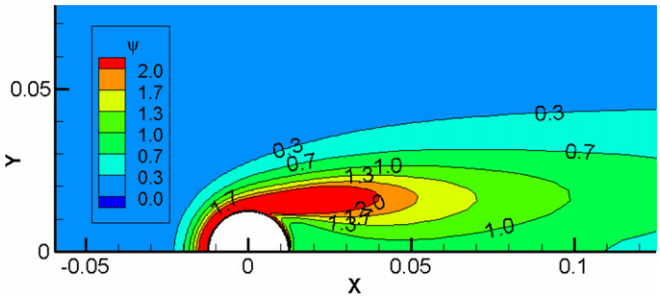

Fig. 3. Ratio of eddy to mean flow time scales (ψ) For the LS k–ε model and $Re_W = 2500$.

(Frame (d)); Secundov's v_t-92 (Frame (e)); k–ε of Chien (Frame (f)) and k–ε based EASM of Abid (Frame (g)). Partly, to save space, contour plots for the following two equation models are not shown: cubic, k–ω, Menter-SST, LS, AKN EASM and AKN k–ε. This is because, with the exception of the cubic, these two equation results look virtually identical to the Frame (g) results. The local eddy viscosity is normalized by the maximum μ_t well upstream of the cylinder.

With the exception of the cubic, the frames (f) and (g) results are the most strikingly different of the two equation results. Broadly speaking, Fig. 4 shows that major qualitative differences are a function of the number of equations solved for in the turbulence model. The ML and k–l models both give strong turbulence production in the wake region resulting in, especially for the k–l model, a very substantial increase in μ_t in this zone. The LVEL and Secundov v_t-92 (and, although not shown, v_t–L) models probably correctly show relatively little cylinder influence. On the other hand, the SA (Frame (d)), k–ε of Chien (Frame (f)), k–ε based EASM of Abid (Frame (g)), k–ω, Menter-SST, LS k–ε, AKN EASM and AKN k–ε suggests the cylinder gives a turbulence deficit in the wake region of over 25%.

The over prediction of eddy viscosity for the k–l model (and also to an extent the ML) and under prediction for the two-equation models (with the exception of the v_t–L) can be explained using Fig. 5. This shows contours of the predicted near cylinder turbulence length scales and flow streamlines for the k–l and LS k–ε models with $Re_W = 2500$. Frame (a) is for the k–l model and (b) for the k–ε. For the k–l model the near cylinder turbulence length scale (see Frame (a)) is governed by the algebraic predominantly wall distance based prescription. Hence, sensitivity to the relatively large free stream turbulence length scales is lost and the predicted stagnation zone l values are small. Therefore, since $\mu_t \sim l$, in the *stagnation zone* of the cylinder μ_t is much lower than for the k–ε model. This appears to result in less aerodynamic resistance and considerably higher (circa 50%) local velocities at the lateral cylinder faces. For the k–ε model (see Frame (b)) the zone of high turbulence dissipation $\sim 1/l$, correctly, is aligned with the streamlines and hence shear layers thus assisting to lower the wake eddy viscosity. However, for

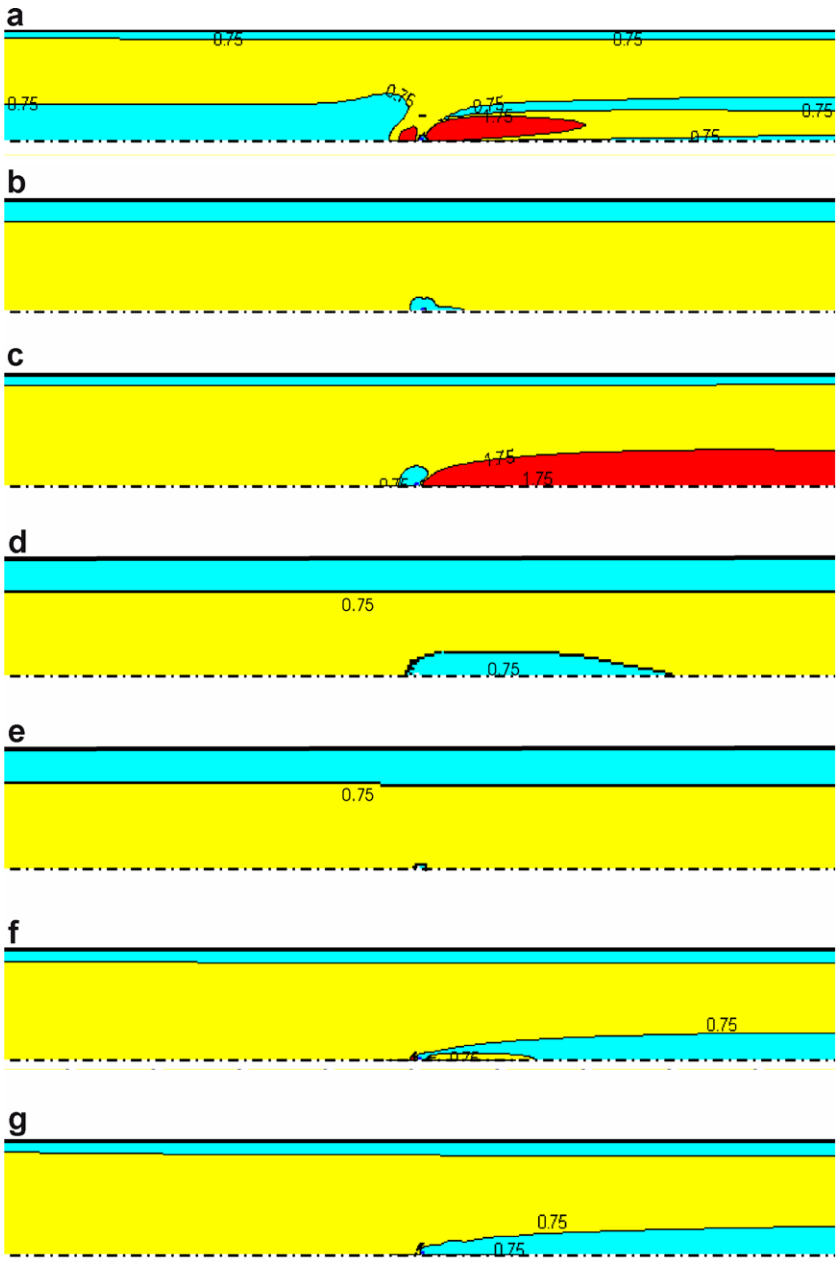

Fig. 4. Dimensionless turbulent viscosity contours for $Re_W = 2.5 \times 10^3$ and the following models: (a) ML; (b) LVEL; (c) k–l; (d) SA; (e) Secundov's v_t-92; (f) k–ε of Chien and (g) k–ε based EASM of Abid et al.

the k–l model, the combination of higher lateral velocities, misalignment (to the extent of near orthogonality) of the lines of effectively constant dissipation with respect to the streamlines along with the higher (algebraically set) channel width based turbulence length scales, well downstream of the cylinder, results in considerably higher wake eddy viscosity levels.

For both the LVEL and ML models, for distances away from the cylinder greater than $H/2$, the turbulence model terms are directly functionally related to just the channel walls (not the cylinder). Hence, beyond this range, any cylinder influence must come from distortions to the mean velocity field. However, as can be partly inferred from results this velocity distortion is fairly minimal and localized (for example, see Fig. 6 later). Hence, as can be seen from Frames (a) and (b) the wire influence is relatively localized. There being little evidence of any μ_t field disturbance extending substantial distances downstream of the cylinder, as there is for the less algebraic equation dominated models. Unlike the ML, the LVEL model does not involve explicit differentiation of the computed velocity field (see Eqs. (A.1) and (A.2)). With LVEL an expected turbulent boundary layer velocity profile form (from a Taylor series fit to the 'law of the wall') is analytically differentiated to infer μ_t. This appears to desensitize the model to the localized rapid flow field strains induced by the cylin-

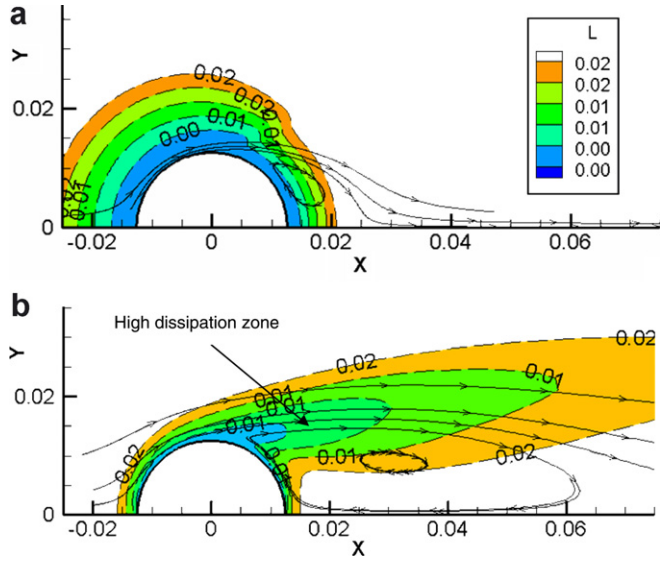

Fig. 5. Contours of the predicted near cylinder turbulence length scales and flow streamlines for the k–l and LS k–ε models with $Re_W = 2500$: (a) k–l model and (b) LS k–ε model.

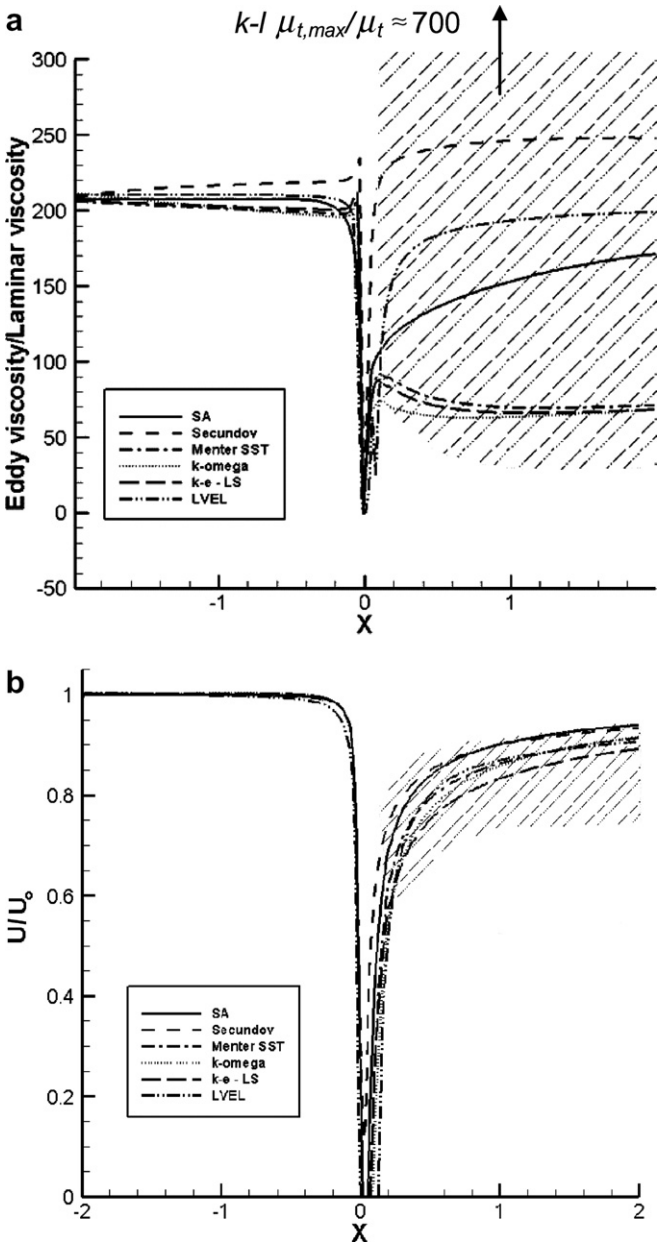

Fig. 6. Streamwise variation at the channel centreline of dimensionless eddy viscosity and streamwise velocity for $Re_W = 2.5 \times 10^3$ and the following models: SA; Seconduv v_t-92; Menter SST; k–ω; *LS* and LVEL: (a) μ_t/μ and (b) U/U_0.

der. This is reflected in the μ_t field being much less disrupted. In its full form the LVEL also exaggerates the wall distance. This would also diminish the cylinder influence. However, in Frame (b), for illustrative purpose the usual wall distance is used. As can be seen from Frame (d), the SA model's turbulence destruction term, which involves a tortuous function of d (see Eq. (11)) clearly ensures the cylinder has a substantial influence. For both of the Secundov models most of the destruction term scales as $1/d$ a 3rd element scaling as $1/d^2$ but multiplied by $\mu/(\mu_t + 0.1\mu)$. The $1/d$ scaling appears to allow elevation of μ_t which even further diminishes the $1/d^2$ element.

Like the other k–ε based models, the cubic shows a significant wake turbulence deficit. However, unlike the other k–ε based models, the cubic gives a significant eddy viscosity drop upstream of the wire. It is worth noting that the cubic model does well for a range of canonical flow tests (see Liu, 2004). A possible explanation for the model traits here is the effect of the square cylinder sharp corners – the model not being tested for a circular cylinder. A revised formulation to remedy sharp corner influences is given by Craft et al. (1999).

Fig. 6 gives more quantitative $Re_W = 2.5 \times 10^3$ turbulent viscosity information along with velocity data. The figure plots μ_t/μ (Frame (a)) and U/U_0 (Frame (b)) against streamwise direction at the channel centerline. Fig. 6 gives results for the following models: LVEL, SA, Secundov's v_t-92, LS k–ε, k–ω and Menter-SST. The shaded regions give the extent of the curve envelope when all the models discussed in this paper are plotted. Partly to save graph overcrowding all these curves are not explicitly plotted. As might be expected from Fig. 4, in Frame (a), a wide range (over 100% variation when considered relative to the inlet values) of turbulent viscosity levels is evident in the downstream region. However, as shown by Frame (b), the velocity field shows a high degree of insensitivity to the eddy viscosity. It is this feature that strongly accounts for the success of RANS models in general engineering simulations. With the standard k–ω model, the Schmidt number in the k transport equation is 0.5. Altering this to the standard Menter SST value has insignificant influence on results.

Fig. 7 plots streamlines and velocity contours for the SA model with $Re_W = 2500$. The top image is for the round cylinder and lower the square. Despite more subtle differences (e.g. the recirculation on the horizontal face of the

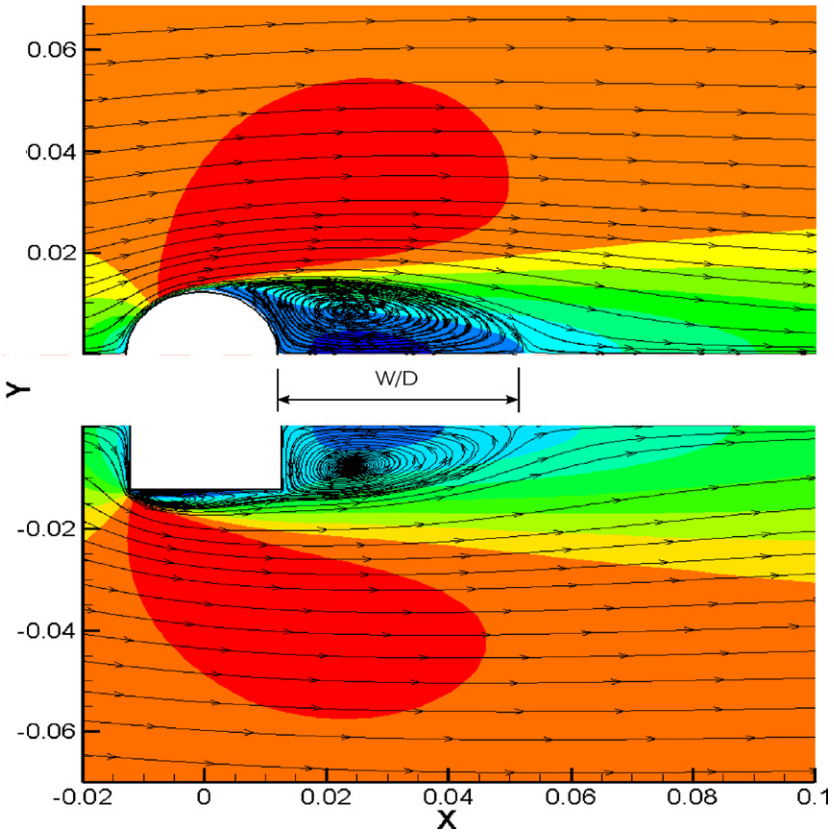

Fig. 7. Plot of streamlines and velocity contours for SA model with $Re_W = 2500$. The top image is for the round cylinder and lower the square.

square cylinder) the gross flow features seem remarkably similar. Both cylinders exhibit a separation bubble of about two cylinder widths, again the level of agreement being remarkably close and perhaps partly fortuitous. The stagnation zone with extreme streamline curvature ahead of the cylinder is evident.

Fig. 8 plots streamlines and velocity contours for k–l model with: (a) $Re_W = 25$ and (b) $Re_W = 0.25$. As with other models, as $Re_W \to 0$ the separation bubble vanishes. However, the trend is not necessarily monotonic. This can be seen by referring back to Fig. 5a, where for $Re_W = 2500$ W/D is clearly shorter than for $Re_W = 25$. However, the broad trend of decreasing W/D with Re_W is obviously to be expected. As noted earlier, the relatively large eddies approaching the cylinder become so rapidly strained that there physics is expected to be governed by linear stress equations. Hence, they are expected to behave like strained solids where linear deformations can be undone. Hence, for frame (b), an eddy approaching the cylinder will experience a sudden strain and the release of this strain as the eddy passes the wire. Hence, based on the rapid distortion theory we would expect symmetry of the turbulence field either side of the cylinder about the y axis. As will be seen later, for the k–l model this symmetry can occur, but by then the cylinder diameter is so small that $y+ = 5$ corresponds to several cylinder diameters. Hence the rapid straining zone does not occur where the flow can be considered turbulent. For the two equation models (except the v_t–L) as $Re_W \to 0$ again there is local symmetry of the flow and turbulence field but this again occurs where the flow is not truly turbulent i.e. in the viscous sublayer and buffer regions. Where the flow is fully turbulent symmetry is lost. Hence, no correspondence with rapid distortion behavior can be found.

Fig. 9 plots dimensionless separation bubble length (W/D) against Re_W and $Re_{W,eff} = \rho U_0 D/(\mu + \mu_{t,ave})$ where $\mu_{t,ave}$ is a linear estimate of the average eddy viscosity around the perimeter of the separation bubble. The diamond symbols give the measurements of Acrivos et al. (1968) the open circles the data of Taneda (1956). The open triangles give laminar flow NEAT computations for a circular cylinder with trimmed cell modeling. The closed circles are for the RANS models based on $Re_{W,eff}$ but with $Re_W = 2500$. The dashed line is a best fit to the Acrivos et al./Taneda data. The full line is the best fit to the RANS based $Re_{W,eff}$ data. Although there is considerable scatter in the RANS results comparison of the lines shows the clear increasing separation bubble length trend with increasing effective Reynolds number. It seems worth noting that the two most extreme data points from this trend are for the simplest models – the ML and LVEL. These points are labeled on the graph. Of course, we would hope that all RANS models gave a consistent W/D. However, since the eddy viscosity changes the effective Reynolds number

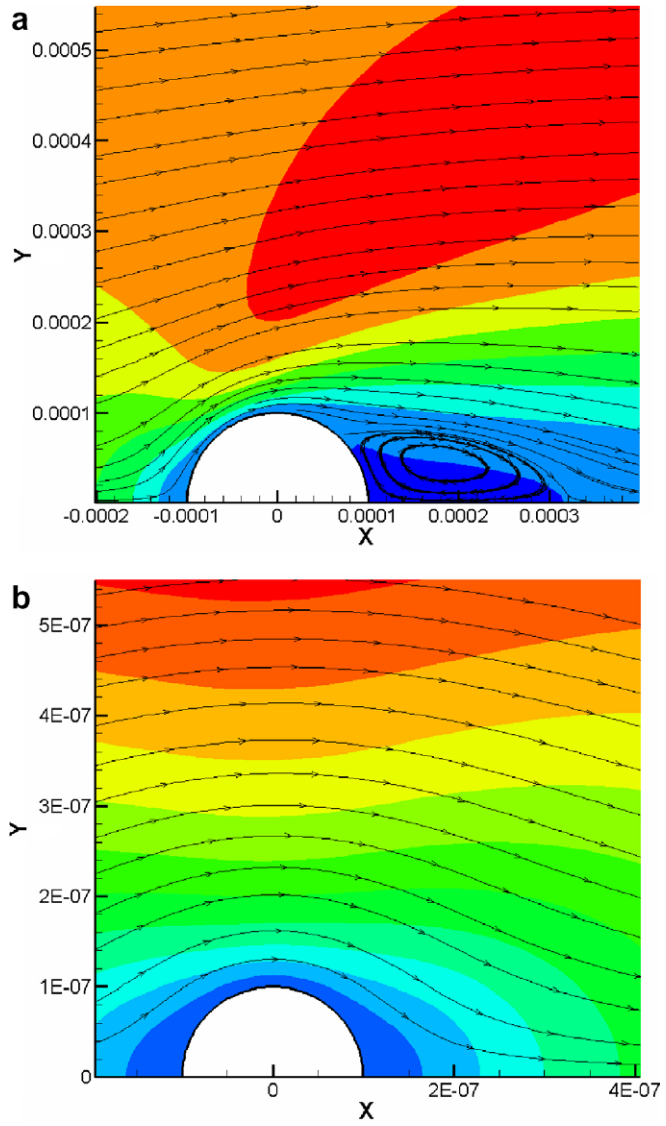

Fig. 8. Plot of streamlines and velocity contours for k–l model with: (a) $Re_W = 25$ & (b) $Re_W = 0.25$.

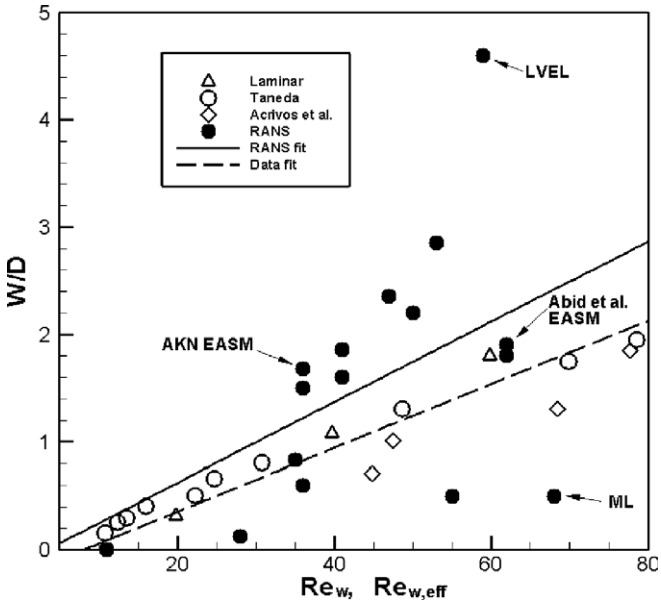

Fig. 9. Plot of dimensionless separation bubble length (W/D) against Re_W & $Re_{W,eff} = \rho U_0 D/(\mu + \mu_{t,ave})$ where $\mu_{t,ave}$ is a linear estimate of the average eddy viscosity around the perimeter of the separation bubble (RANS results for $Re_W = 2500$).

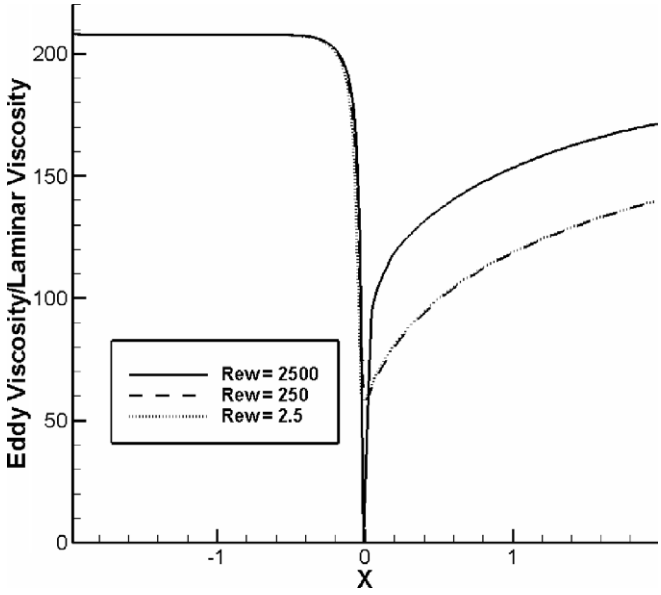

Fig. 10. Plot of μ_t/μ against streamwise direction at the channel centerline for SA and $Re_W = 2.5$, 250 and 2500.

of the flow this hope cannot be realized. Nonetheless, it seems worth pointing out that the non-linear models, that are less reliant on eddy viscosity, show less $Re_{W,eff}$ dependence. For example, the AKN EASM and Abid et al. EASM, labeled on the graph, have similar W/D values, these being, like the cubic model's, at around 2.

Fig. 10 plots μ_t/μ against streamwise direction at the channel centerline for SA and $Re_W = 2500$, 250 and 2.5. A key thing to notice is that for SA the order of magnitude cylinder diameter *decrease* from $Re_W = 2500$ to 250 unexpectedly *strengthens* the cylinder influence. Also, as can be seen from the subsequent two orders of magnitude reduction in cylinder diameter to go from $Re_W = 250$ to 2.5, no matter how small the cylinder, its influence is strong and does not vanish, the $Re_W = 250$ and 2.5 results overlaying. Perhaps the key reason for this is that the turbulence destruction term relies on a complex wall distance related function with d raised to high powers. Also, the foot print of d never vanishes, no matter how small the cylinder. It seems worth pointing out here that the SA model generally gives disappointing results for shear layer flows like jets. This is because it is not designed for such flows. Remedying the SA model's under prediction of μ_t in shear layers the v_t-92 and v_t–L models have additional productions terms (see underlined terms in Eqs. (A.8) and (A.12)), the modelers having aspirations to develop equations suitable for a wider range of flows. The above noted added production terms for the v_t-92 and v_t–L models will elevate μ_t in

the wake region, potentially masking the cylinder's excessive disruptive influence. The addition of similar production terms to SA, as well as improving accuracy for jets, could yield more plausible results for the current flow.

Fig. 11 plots μ_t/μ against streamwise direction at the channel centerline for the k–l model and $Re_W = 2$ to 2500. Clearly, as shown in Fig. 4, for $Re_W = 2500$ the model gives a dramatic over prediction of wake eddy viscosity. However, the cylinder influence, as with both the Secundov models, correctly diminishes with decreasing Re_W. Nonetheless, for $Re_W = 2500$, μ_t is considerably higher than if there had been no cylinder. Clearly under these circumstances the exaggeration of d would not palliate the excessive cylinder influence problem, instead making results worse. Hence, it is clear that care is required in modifying the distance function to remedy turbulence models defects. Clearly, the distance function must be customized to both the turbulence model and flow physics.

As with Fig. 11, for the LS k–ε model, as for other two equation models tested the cylinder influence *correctly* appears to diminish with decreasing cylinder size (down to $Re_W = 2.5$). However, the rate of diminishment is surprisingly slow. Also, it is difficult to secure iterative convergence as $Re_W \to 0$ and hence confirm if the cylinder influence totally vanishes. It seems worth noting here that the standard Menter SST model is especially difficult to converge for small Re_W. Also, the model appears have little influence in the adverse pressure gradient wake region where some influence might be expected from the SST terms. However, removal of the SST element greatly improves convergence. This instability might be related to the hyperbolic tangent function based SST activation term which includes a $1/d^2$ element. Also, little difference was found between wake eddy viscosity levels for the two versions of k–ω model considered. Fig. 12 plots μ_t/μ against streamwise direction at the channel centerline for the LS k–ε and different levels of inlet turbulence intensities. Upstream of the wire, the eddy viscosity for the higher inlet intensity again shows a slow decay. Clearly the inlet intensity has little influence (a maximum difference in μ_t of about 7%) on the turbulence level down stream of the cylinder along its centerline. This suggests there is little diffusion of the relatively high ambient turbulence intensity into the wake region.

Fig. 13 supports this view plotting dimensionless streamwise velocity U^* against the dimensionless y coordinate, ξ, at $x/D = 75$ for different turbulence models and $Re_W =$

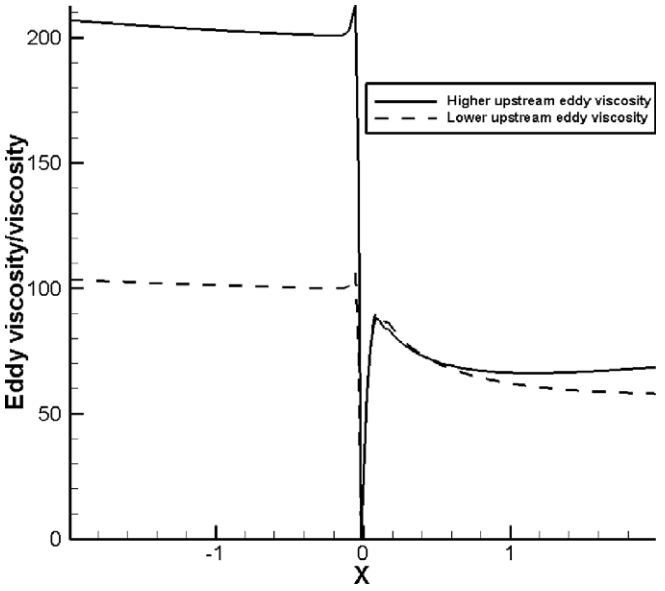

Fig. 12. Plot of μ_t/μ against streamwise direction at the channel centerline for the LS k–ε and different levels of inlet turbulence intensities (corresponding to $\mu_t/\mu \approx 100$ and 200).

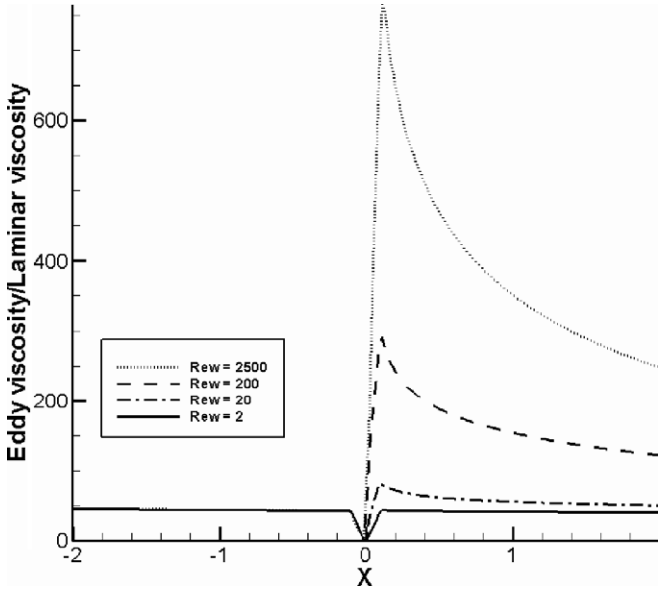

Fig. 11. Plot of μ_t/μ against streamwise direction at the channel centerline for the k–l model and $Re_W = 2$ and 2500.

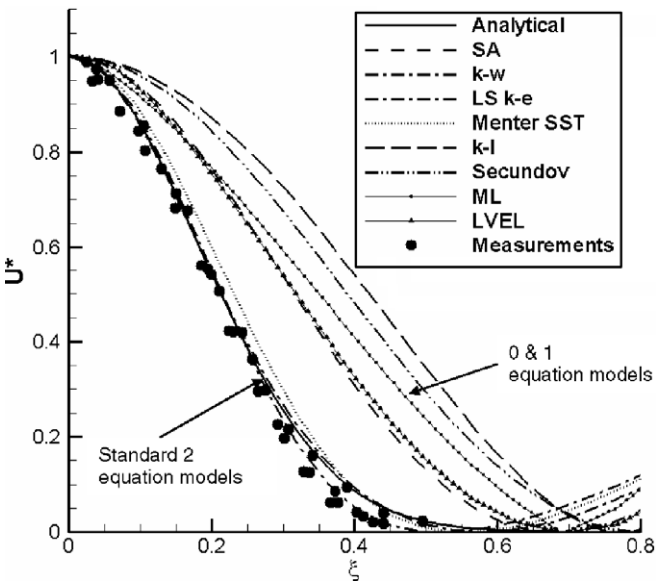

Fig. 13. Plot of dimensionless streamwise velocity against dimensionless y coordinate at $x/D = 75$ for different turbulence models and $Re_W = 2500$.

2500. The dimensionless axial velocity $U^* = (U_{max} - U)/(U_{max} - U_{min})$ where U_{min} is the minimum velocity. Also, the dimensionless y coordinate $\xi = y/\sqrt{Dx}$. The symbols are measurements (see Hinze, 1975). The full line is an analytical curve. All the standard two equation models (Menter SST, k–ω, LS k–ε) show close agreement with the measurements and theory. This supports the Fig. 12 data which suggests that the external turbulence has little influence on the predicted wake mean flow behavior. Notably, of the two equation models v_t–L predicts no wake zone – hence this curve is omitted from the figure. As can be see from Fig. 13 the zero and one equation models predict spreading of the Gaussian wake. On physical grounds this is to be expected. However, the occurrence of this spreading in the computations seems largely fortuitous in modeling terms.

3.2. Distance function's traits and influence on cylinder's wake region

Fig. 14 plots μ_t/μ against streamwise direction at the channel centerline for the SA model and $Re_W = 2500$. The full line is for d based on the search procedure. The dashed line gives results when the Poisson based $\tilde{d}$ is used. Clearly the latter, which exaggerates the wall distance and hence turns off the turbulence destruction term (see Eq. (10)), gives more plausible results suggesting the wire/cylinder has a negligible influence.

Fig. 15 plots the Poisson $\tilde{d}$ variation against distance from the cylinder when the cylinder is placed in an infinite domain. Curves corresponding to the three Re_W considered here are plotted. As can be seen the distance overestimation increases with decreasing Re_W (essentially cylinder diameter - since the equation is not sensitized to flow conditions). Observation of Fig. 10 would suggest that broadly this trait

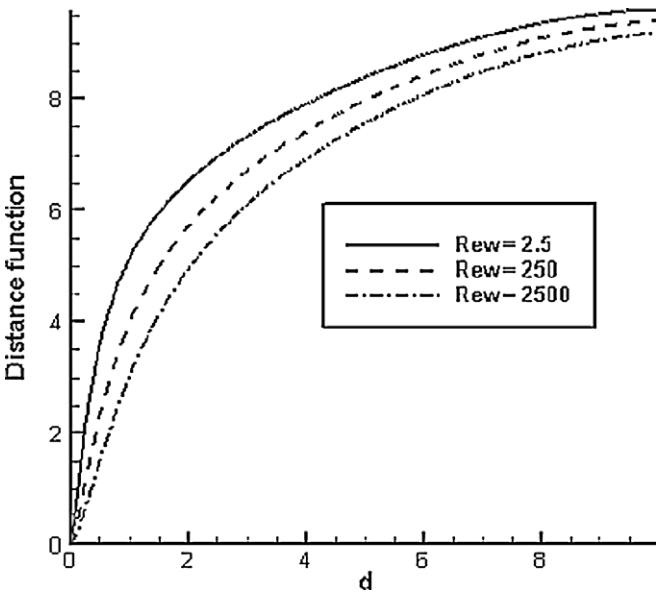

Fig. 15. Poisson $\tilde{d}$ variation against d for cylinder diameters corresponding to $Re_W = 2500$, 250 and 2.5 in an infinite environment.

is desirable for the SA model. As just noted, overestimating the actual distance reduces the SA model's turbulence destruction. Clearly, to get the correct limiting behavior (i.e. as the cylinder diameter tends to zero it should have no flow influence) with decreasing Re_W (wire/cylinder diameter) the d over-estimation should increase.

Fig. 16 gives the variation of $\tilde{d}$ with d around the cylinder for the Eikonal (full line), HJ (long dashed line) and Poisson (short dashed line) equations when they are evaluated in the channel geometry. For reference purposes the chain dashed line gives the infinite domain Poisson equation $\tilde{d}$ distribution. The HJ line uses Eq. (8) with $\varepsilon = 8$. The key thing to notice from this figure is that for $\varepsilon = 8$

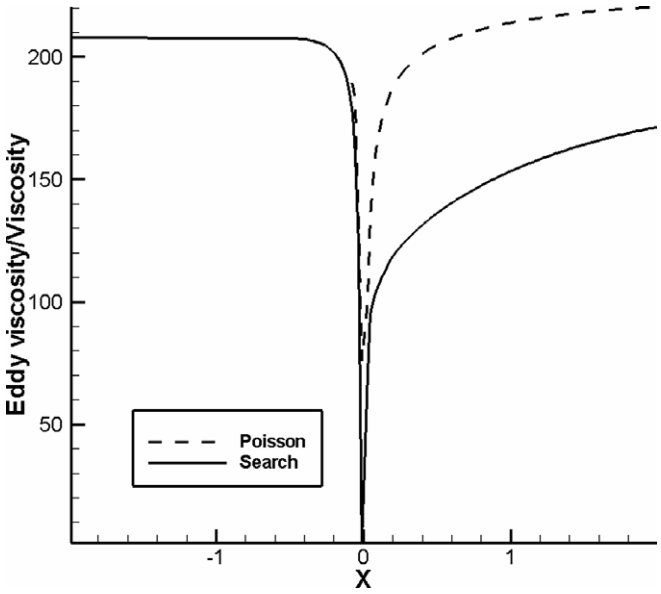

Fig. 14. Plot of μ_t/μ against streamwise direction at the channel centerline for SA, $Re_W = 2500$ and the search and Poisson based distance values.

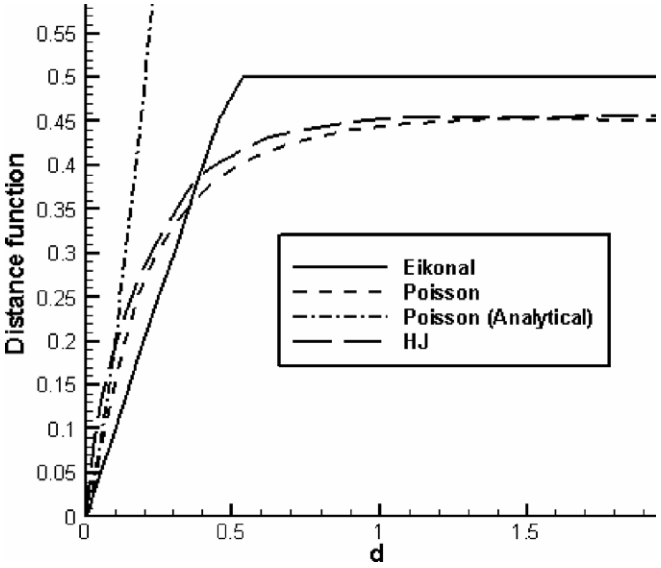

Fig. 16. Variation of $\tilde{d}$ with d for the Eikonal, HJ and Poisson equations in the channel geometry.

the HJ and Poisson $\tilde{d}$ distributions are within 5% of each other. Also, as for the Poisson equation, as $D \to 0$ the HJ's Laplacian term strengthens and the d overestimation is exaggerated. Hence, when using the HJ equation the beneficial behavior observed in Fig. 14 can also be gained.

3.3. Cylinder results for stagnation region

Fig. 17 compares the eddy viscosity ratio, $\mu_t/\mu_{t,max}$, upstream of cylinder for various models when $L/D \approx 2$ (Note, the estimate for L is based on the expected mixing length for a fully developed channel flow). In the ratio definition $\mu_{t,max}$ is taken as the maximum centre-line value upstream of $(x/D > 2)$ the cylinder. The symbols essentially give the measurements of Britter et al. (1979) as processed by Maslov et al. (1999). The processing procedure involves estimating the eddy viscosity ratio as $\mu_t/\mu_{t,max} = (u'L)/(u'L)_{max}$ where $(u'L)_{max}$ represents free stream conditions. Frame (a) contrasts performances of the single equation, essentially μ_t transport equation based, SA and v_t-92 models along with the extended two-equation version of v_t-92 i.e. v_t–L. As would be expected (see Secundov et al., 2001), the two equation Secundov et al. model (represented by the full line), gives better results than the single equation version, represented by the chain dashed line. Hence it appears the L equation in the two equation version is sensibly sensitized to the effect of wall proximity on L, the equation modeling having a sufficiently elliptic nature. Nonetheless, the single equation SA model's accuracy, despite not having any information about the free stream turbulence length scales, is not dissimilar to that of the two equation v_t–L. Frame (b) further explores the SA model's performance, contrasting it when used with its curvature and rotation correction (dashed line). Clearly the Poisson distance function improves the SA models stagnation region performance (see chain dashed line) more than using its SARC form. Also, it is worth noting that despite giving some, apparently useful, sensitization to the strong streamline curvature ahead of the cylinder, in the wake region SARC is found unhelpful.

Frames (c) and (d) essentially explore the stagnation region performances of the ML, LVEL and k–l models when the exact (search) and Poisson distance fields are used. Frame (c) gives the ML model results, the full and dashed lines being for the exact and Poisson distance fields, respectively. Frame (d) gives k–l and LVEL results, the dotted and chain dashed lines being for these models, respectively, with exact d fields. The k–l and LVEL results using the Poisson $\tilde{d}$ fields are represented by the full and dashed lines, respectively. Clearly, as with SA, the Poisson $\tilde{d}$ considerably improves results for the ML, LVEL and k–l models. Exaggeration of d for the k–l model will correctly give dominance to the large upstream turbulence length scales which are of key importance in the stagnation zone (as noted by Secundov et al. (2001), a thick layer which scales with the free stream turbulence length scale exists around the stagnation line). Hence, this modeling improvement seems reasonable. However, as noted earlier, the d exaggeration worsens the wake region modeling. For the ML and LVEL models again the diminishment of the cylinder's control of the stagnation zone turbulence length scales seems sensible. However, there is no convective modelled length scale element relating to the free stream and so any accuracy improvements lack rational basis.

Frames (e) and (f) focus on the two-equation model performances. Frame (e) presents the LS, LS with the Yap correction, LS with the Kato and Launder correction and AKN, k–ε based models using chain dashed, dashed, full and dotted lines, respectively. Frame (f) gives the k–ε based EASMs of Abid et al. and AKN along with the Menter SST and k–ω models using full, dashed, chain dashed and dotted lines, respectively. As can be seen most of the two equation models give unphysical maxima. For many models, the maxima corresponds to around a 50% overprediction in v_t. As noted by Secundov et al. (2001), the stagnation zone boundary layer is functionally related to the free stream turbulence length scale and not turbulence intensity. Furthermore, for the k–ε model there is excessive dominance of the convective term. According to Secundov et al. this causes the peak in μ_t and hence excessive predicted heat transfer found in studies by other workers. As pointed out by Kato and Launder (1993) a remedy is to replace the strain rate based production term with a more vorticity based term (see Eqs. (17) and (18)) – vorticity being very nearly zero in stagnation zones. As can be seen from Frame (e) this is clearly helpful.

As can also be seen from Frame (e), use of the Yap correction with the LS model is found to have an insignificant effect on the eddy viscosity ratio. The Yap term is intended to remedy excessively high predicted turbulence length scales for the k–ε model. Where the ratio of the predicted length scale to the local equilibrium length scale is greater than unity the correction will increase the predicted dissipation. Craft et al. (1999) found the Yap correction helpful in stagnation zones however, surprisingly, it has little influence here. As noted earlier, the cubic model is found to dramatically under-predict the eddy viscosity in the cylinder vicinity (which has sharp corners) suggesting the Craft et al. (1999) cubic model formulation is required. The Chien k–ε model has the reverse trait to the cubic. Saving space these anomalous results are not plotted. However, it is worth noting that surprisingly the Poisson d field significantly improves the Chien result. Nonetheless the peak in eddy viscosity at around $x/D \approx 2$ is still about 50% greater than that for the LS model. As would be expected, since for the k–ε model results, generally the stagnation region turbulence is too high, overestimating d is unhelpful.

3.4. Airfoil results for wake region

Poisson and exact d results are now compared for the trailing edge region of the NACA4412 airfoil. The attack angle is 13.87°, the Mach number 0.2 and

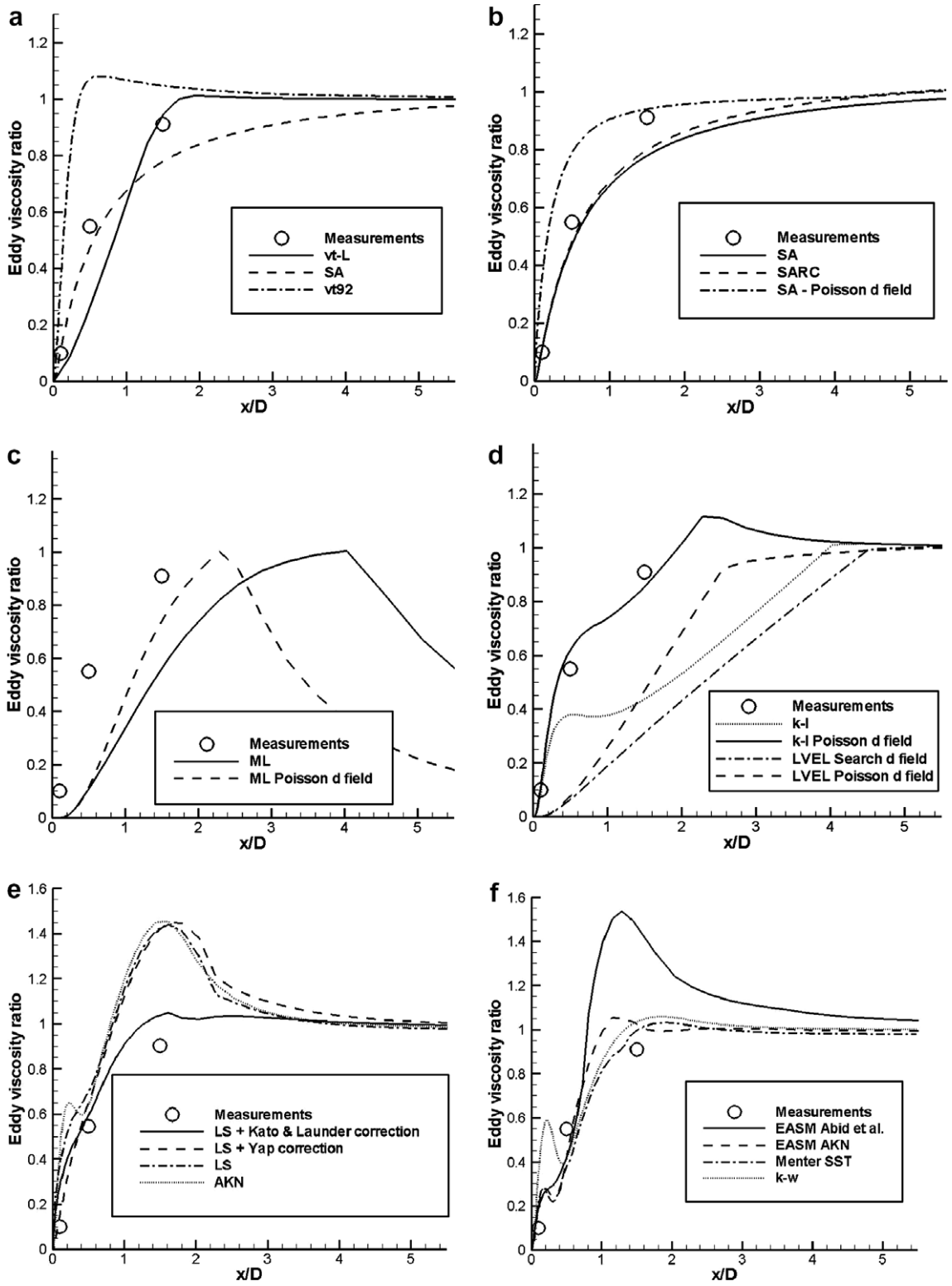

Fig. 17. Eddy viscosity ratios on the centerline upstream of cylinder for $L/D \approx 2$ and the following models: (a) v_t–L, v_t-92 and SA; (b) SA, *SARC* and SA with Poisson $\tilde{d}$ function; (c) ML and ML with Poisson $\tilde{d}$ function; (d) k–l, k–l with Poisson $\tilde{d}$ function, LVEL and LVEL with Poisson $\tilde{d}$ function; (e) LS, LS with Kato and Launder correction, LS with Yap correction and AKN; (f) *EASM* of Abid et al., EASM AKN, Menter SST and k–ω.

$Re = 1.52 \times 10^6$ (based on the wing chord, c). Fig. 18 gives SA model, trailing edge region, turbulent viscosity contours for exact (Frame (a)), and Poisson (Frame (b)) distances. The larger $x/c > 1$ ($x = 0$ corresponds to the wing leading edge) Poisson distances, reduce the modeled turbulence destruction and so increase μ_t by just under 5%.

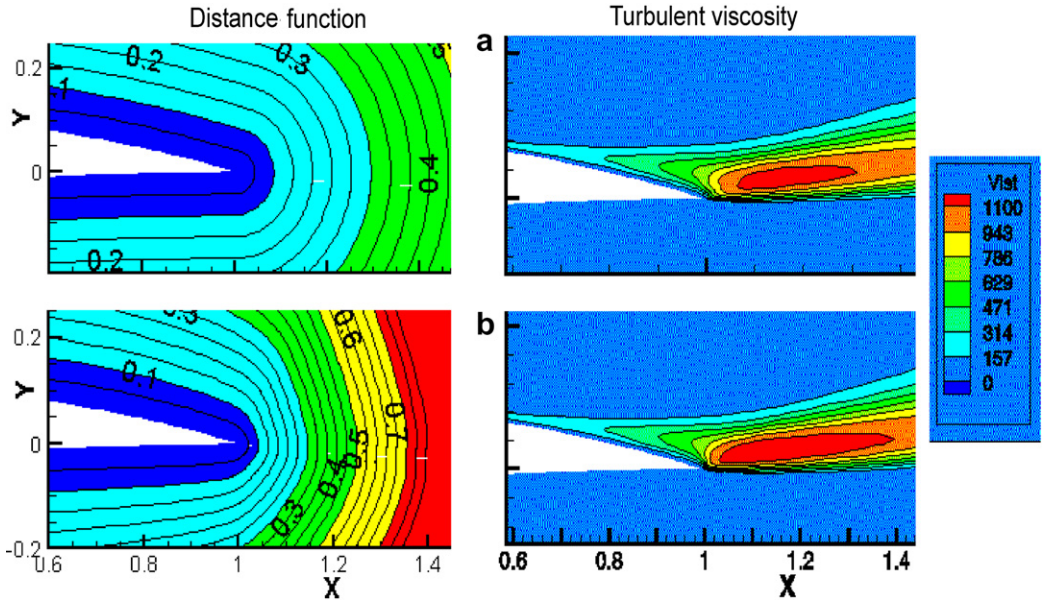

Fig. 18. Turbulent viscosity contours for NACA4412 airfoil at an angle of attack of 13.87°, a Mach number of 0.2 and $Re = 1.52 \times 10^6$ (based on chord): Exact distance field and (b) Poisson $\tilde{d}$ field.

Fig. 19 compares predicted normal stresses with the measurements of Coles and Wadcock (1979) at $x/c = 1.1$. The dashed line gives results for the Eikonal equation. These will be virtually the same as those obtained for a correct search procedure. The full line gives the Poisson equation results. Clearly, these give a higher normal stress. The global lift and drag coefficients are virtually identical (on average circa 1% variation) for the two distance fields. However, clearly, the different d fields could have implications for multi-element systems where downstream elements will encounter significantly different 'free stream' eddy viscosity levels. Hence, it seems the wall distance and its traits should be considered an integral part of a distance based RANS model. As noted by Tucker et al. (2005), with multi-element airfoils, minor changes in upstream turbulence conditions can lead to non-unique solutions.

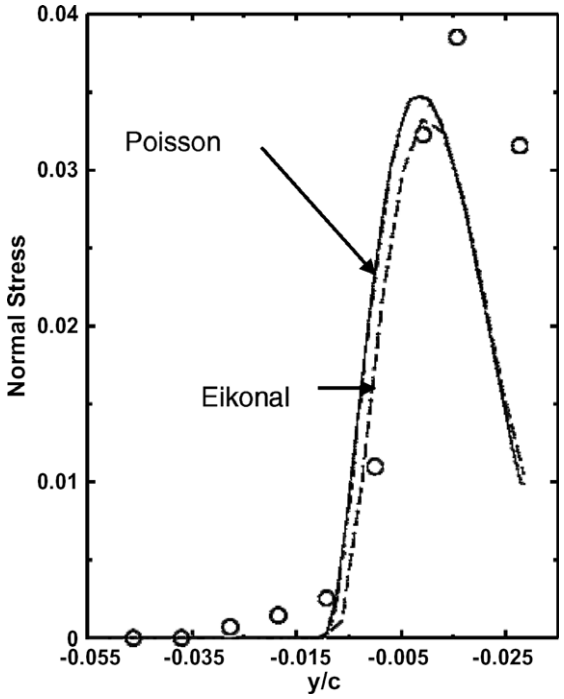

Fig. 19. Normal stress distributions at $x/c = 1.1$ for NACA4412 airfoil at an angle of attack of 13.87°, a Mach number of 0.2 and $Re = 1.52 \times 10^6$ (based on chord) with exact and Poisson $\tilde{d}$ fields.

4. Conclusions

For the small cylinder (wire), the RANS models showed significantly different predictive traits. The mixing length and k–l models gave excessively strong turbulence production in the wake region. However, in accord with eddy viscosity estimates (i.e. more correctly), the *LVEL* and Secundov ν_t-92 models showed relatively little cylinder influence. On the other hand, two equation models suggested the cylinder wrongly gave a strong turbulence deficit in the wake region. Unlike the other one equation models, SA also showed this deficit trait. Also, for SA, an order or magnitude cylinder diameter decrease from $Re_W = 2500$ to 250 erroneously strengthened the cylinder influence rather than weakened it as it should. Importantly, results for $Re_W \gg 250$ were virtually identical to those for $Re_W = 250$ i.e. no matter how small the cylinder its influence did not vanish. Similar tests for the Launder–Sharma k–ε, Menter SST and k–ω models showed, in accordance with physical reality, that the cylinder's influence diminishes (but surprisingly slowly) with decreasing size. Results suggested the Poisson and Hamilton–Jacobi equation distance functions palliate the SA model's erroneous trait.

For stagnation line eddy viscosities upstream of cylinder the Poisson distance function improved the zero and one-equation model results. Poisson and exact wall distance results were compared for the sharp convex trailing edge region of an airfoil. The larger Poisson distance function increased the wake region turbulence by just under 5% again improving agreement with available measured data.

Acknowledgements

The work was carried out at the University of Wales, Swansea. The financial support from the UK Engineering and Physical Sciences Research Council (EPSRC) under grant number GR/T06629/01 is greatly appreciated. We would also like to thank M. Shur for use of the excellent NTS code. Also, we are grateful to P.R. Spalart for helpful discussions.

Appendix

1. Spalding's LVEL model

This is a one equation model that uses the following Taylor series based fit to the 'law of the wall'

$$y^+ = u^+ + \frac{1}{E}\left[e^{0.4u^+} - 1 - \frac{\kappa u^+}{1!} - \frac{(\kappa u^+)^2}{2!} - \frac{(\kappa u^+)^3}{3!} - \frac{(\kappa u^+)^4}{4!}\right] \tag{A.1}$$

In the above $u^+ = U\sqrt{\rho/\tau_W}$, $\kappa = 0.4$ and $E = 9.0252$. After differentiating Eq. (A.1) and rearranging, the following turbulent viscosity expression is gained

$$\mu_t = \mu\frac{\kappa}{E}\left[e^{\kappa u^+} - 1 - \frac{\kappa u^+}{1!} - \frac{(\kappa u^+)^2}{2!} - \frac{(\kappa u^+)^3}{3!}\right] \tag{A.2}$$

Spalding (1994) intended the Poisson distance function to be an integral part of the LVEL model.

2. SARC model

With the SARC model (Spalart and Shur, 1997), a portion of the SA model's production term, $C_{b1}(1 - f_{t2})W\tilde{\nu}$, is replaced by $C_{b1}(f_{r1} - f_{t2})W\tilde{\nu}$, where f_{r1} is expressed as

$$f_{r1}(r^*, \tilde{r}) = (1 + c_{r1})\frac{2r^*}{1 + r^*}[1 - c_{r3}\tan^{-1}(c_{r2}\tilde{r})] - c_{r1} \tag{A.3}$$

In the above the dimensionless quantity, r^* is defined as

$$r^* = S/\Omega \tag{A.4}$$

where S and Ω are as given by Eq. (17). Ignoring terms relating to reference frame rotation the quantity $\tilde{r}$ is defined below as

$$\tilde{r} = \frac{2\omega_{ik}S_{jk}}{D^4}\frac{DS_{ij}}{Dt} \tag{A.5}$$

where DS_{jk}/Dt are the components of the Lagrangian derivative of the strain rate tensor. The vorticity tensor in Eq. (A.5) is defined as below

$$\omega_{ik} = \frac{1}{2}\left[\left(\frac{\partial U_i}{\partial x_k} - \frac{\partial U_k}{\partial x_i}\right)\right] \tag{A.6}$$

and

$$D = \sqrt{0.5(S^2 + \Omega^2)}$$

Finally, the model constants in Eq. (A.3) are as follows: $C_{r1} = 1.0, C_{r2} = 12$ and $C_{r3} = 1.0$.

3. The ν_t-92 model

The transport equation for the kinematic turbulent viscosity, $\nu_t(\nu_t = \mu_t/\rho)$, takes the following form:

$$\frac{\partial \nu_t}{\partial t} + \frac{\partial u_i \nu_t}{\partial x_i} = \frac{\partial}{\partial x_i}\left[(C_0\nu_t + \nu)\frac{\partial \nu_t}{\partial x_i}\right] + \frac{\partial}{\partial x_i}[(C_0 - C_1)\nu_t - \nu]\frac{\partial \nu_t}{\partial x_i} + P_\nu - D_\nu \tag{A.7}$$

where ν is the molecular kinematic viscosity and the difference between the production (P_ν) and dissipation (D_ν) terms is obtained from

$$P_\nu - D_\nu = \underline{C_2F_2(\nu_t\Gamma_1 + A_1\nu_t^{4/3}\Gamma_2^{2/3}) + C_2F_2A_2N_1} \times \underline{\sqrt{(\nu + \nu_t)\Gamma_1} + C_3\nu_t\left(\frac{\partial^2\nu_t}{\partial x_i\partial x_i} + N_2\right)} - C_4\nu_t\left(\frac{\partial U_i}{\partial x_i} + \left|\frac{\partial U_i}{\partial x_i}\right|\right) - \frac{C_5\nu_t^2\Gamma_1^2}{a^2} - \frac{[C_6\nu_tN_1d + C_7F_1\nu\nu_t]}{d^2} \tag{A.8}$$

In the above a is the speed of sound. The functions F_1 and F_2 are computed, respectively, from the expressions below

$$F_1 = \frac{N_1d + 0.4C_8\nu}{\nu_t + C_8\nu}, \quad F_2 = \frac{\chi^2 + 1.3\chi + 0.2}{\chi^2 - 1.3\chi + 1.0} \tag{A.9}$$

where $\chi = \nu_t/(7\nu)$. In Eq. (A.8), the parameters Γ_1, Γ_2, N_1 and N_2 are defined as follows:

$$\Gamma_1^2 = \frac{\partial u_i}{\partial x_j}\left(\frac{\partial u_i}{\partial x_j} + \frac{\partial u_j}{\partial x_i}\right), \quad \Gamma_2^2 = \sum_i\left(\frac{\partial^2 u_i}{\partial x_j\partial x_j}\right)^2,$$
$$N_1^2 = \sum_i\left(\frac{\partial \nu_t}{\partial x_i}\right)^2, \quad N_2^2 = \sum_i\left(\frac{\partial N_1}{\partial x_i}\right)^2$$

The constants in the above equations are: $A_1 = -0.5, A_2 = 4.0, C_0 = 0.8, C_1 = 1.6, C_2 = 0.1, C_3 = 4.0, C_4 = 0.35, C_5 = 3.5, C_6 = 2.9, C_7 = 31.5, C_8 = 0.1$.

4. Two-equation ν_t–L model

For the ν_t–L model, two transport equations are solved. One is for ν_t and the other for the length scale, L. They, respectively, read as follows:

$$\frac{\partial \nu_t}{\partial t} + \frac{\partial u_i \nu_t}{\partial x_i} = [C_0(1+\Phi)\nu_t + \nu]\frac{\partial^2 \nu_t}{\partial} x_i^2 + P_\nu - D_\nu \qquad (A.10)$$

$$\frac{\partial L}{\partial t} + u_i \frac{\partial L}{\partial x_i} = [k_0(1+\Phi)\nu_t + \nu]\frac{\partial^2 L}{\partial x_i^2} + \frac{k_1(1+\Phi)G\nu_t}{L} + \frac{k_2 \nu_t}{L} - \frac{L}{3}\frac{\partial U_i}{\partial x_i} - \frac{k_3 L \nu_t \Gamma_1}{\nu_t + \nu} - \frac{k_4(1+\Phi)G\nu_t L}{d^2} \qquad (A.11)$$

where

$$\begin{aligned} P_\nu - D_\nu &= \underline{C_2F_2(\nu_t\Gamma_1 + A_1\nu_t(\nu_t+\beta\nu)(\nu_t+\nu)^{-2/3}\Gamma_2^{2/3}) + C_2F_2A_2N_1\sqrt{(\nu+\nu_t)\Gamma_1}} \\ &\quad + C_3\nu_t\left(\frac{\partial^2 \nu_t}{\partial x_i \partial x_i} + N_2\right) + \frac{C_1(1+\Phi)\nu_t N_1}{L\left(1+\frac{0.1L^2\Gamma_1}{\nu_t+\nu}\right)} \\ &\quad - C_4\nu_t\left(\frac{\partial U_i}{\partial x_i} + \left|\frac{\partial U_i}{\partial x_i}\right|\right) - \frac{C_5\nu_t^2\Gamma_1^2}{a^2} \\ &\quad - \frac{[C_6(1+C_9\Phi)\nu_t(N_1 d) + C_7F_1\nu\nu_t]}{d^2} \end{aligned} \qquad (A.12)$$

In the above $G^2 = (\partial L/\partial x_i)^2, \Phi = K(L^2/\nu_t)\partial L/\partial x_i S_{ik}\partial L/\partial x_k$. The constants in Eqs. (A.10)–(A.12) are: $A_1 = -0.5$, $A_2 = 4.0, C_0 = 0.8, C_1 = 2.6, C_2 = 0.1, C_3 = 4.0, C_4 = 0.35$, $C_5 = 3.5, C_6 = 3.3, C_7 = 26, C_8 = 0.2 + (0.035\beta)^2, \beta = 10$, $C_9 = 0.1, K = 0.3, k_0 = 0.1, k_1 = 1.6, k_2 = 1.0, k_3 = 0.1$ and $k_4 = 2.6$. The other quantities for this model are the same as in the ν_t-92.

References

Abe, K., Kondoh, T., Nagano, Y., 1994. A new turbulence model for predicting fluid flow and heat transfer in separating and reattaching flows-I. flow field calculation. Int. J. Heat Mass Transfer 37, 139–151.

Abid, R., Morrison, H.J., Gatski, T.B., 1996. Prediction of aerodynamic flows with a new explicit algebraic stress model. AIAA J. 34 (12), 2632–2635.

Acrivos, A., Leal, L.G., Snowden, D.D., Pan, F., 1968. Further experiments on steady separated flows past bluff objects. J. Fluid Mech. 34 (1), 25–48.

Ashforth-Frost, S., Jambunathan, K., 1996. Numerical prediction of semi-confined jet impingement and comparison with experimental data. Int. J. Numer. Methods Fluids 23, 295–306.

Britter, R.E., Hunt, J.C.R., Mumford, J.C., 1979. The distortion of turbulence by a circular cylinder. J. Fluid Mech. 92 (Part 2), 269–301.

Chien, K.Y., 1982. Prediction of channel and boundary layer flows with a low-Reynolds number turbulence model. AIAA J. 20, 33–38.

Coles, D., Wadcock, A.J., 1979. Flying hot-wire study of flow past an NACA 4412 airfoil at maximum lift. AIAA J. 17 (4), 321–329.

Craft, T.J., Launder, B.E., Suga, K., 1996. Development and application of a cubic eddy-viscosity model of turbulence. Int. J. Heat Fluid Flow 17, 108–115.

Craft, T.J., Iacovides, H., Yoon, J.H., 1999. Progress in the use of non-linear two-equation models in the computation of convective heat-transfer in impinging and separated flows. Flow, Turbulence Combust. 63, 59–80.

Dullenkopf, K., Mayle, R.E., 1995. An account of free-stream-turbulence length scale on laminar heat transfer. J. Turbomachinery 117, 401–406.

Fares, E., Schroder, W., 2002. A differential equation to determine the wall distance. Int. J. Numer. Methods Fluids 39, 743–762.

Franke, R., Rodi, W., 1993. Calculation of vortex shedding past a square cylinder with various turbulence models. In: 8th International Symposium of Turbulent Shear Flows, Munich, pp. 189–204.

Hinze, J.O., 1975. Turbulence. McGraw-Hill, Inc.

Hunt, J.C.R., 1973. A theory of turbulent flow around two dimensional bluff bodies. J. Fluid Mech. 61 (part 4), 625–706.

Hunt, J.C.R., 1976. Turbulent velocities near and fluctuating surface pressures on structures in turbulent winds. In: Proceedings of 4th International Conference on Wind Effects on Buildings and Structures, pp. 309–320.

Hussain, A.K.M.F., Reynolds, W.C., 1975. Measurements in fully developed turbulent channel flow. ASME J. Fluids Eng. (December), 568–580.

Kato, M., Launder, B.E., 1993. The modeling of turbulent flow around stationary and vibrating square cylinders. In: 9th Symposium on Turbulent Shear Flows, Kyoto, Japan, pp. 10-4-1–10-4-6.

Launder, B.E., Reece, G.J., Rodi, W., 1975. Progress in the development of a Reynolds-stress turbulence closure. J. Fluid Mech. 68 (part 3), 537–566.

Launder, B.E., Sharma, B.I., 1974. Application of the energy –dissipation model of turbulence to the calculation of flow near a spinning disc. Lett. Heat Mass Transfer 1, 131–138.

Liu, Y., 2004. Numerical simulations of unsteady complex geometry flows. PhD Thesis, School of Engineering, The University of Warwick.

Maslov, V.P., Mineev, B.I., Pichkov, K.N., Secundov, A.N., Vorobiev, A.N., 1999. Turbulence intensity, length scale and heat transfer around stagnation line of cylinder and model blade, ASME Paper 99-GT-423.

Menter, F.R., 1993. Zonal two equation k-ω turbulence models for aerodynamic flows. AIAA Paper AIAA-93-2906.

Mompean, G., Gavrilakis, S., Machiels, L., Deville, M.O., 1996. On predicting the turbulence-induced secondary flows using non-linear k-ε models. Phys. Fluids 8 (7), 1856–1868.

Pan, Z., Tucker, P.G., 2001. Computation of incompressible flow using a Cartesian grid with a boundary cut cell treatment. CFD Journal, Special Number 2001 (Proc. ISCFD'99), pp. 614–621.

Secundov, N., Strelets, M.K., Travin, A.K., 2001. Generalization of νt-92 turbulence model for shear-free and stagnation point flows. J. Fluids Eng. 123 (March), 111–115.

Sethian, J.A., 1999. Level Set Methods and Fast Marching Methods. Cambridge University Press.

Shur, M.L., Spalart, P.R., Strelets, M.Kh., Travin, A.K., 2003. Towards the prediction of noise from jet engines. Int. J. Heat Fluid Flow 24, 551–561.

Spalart, P.R., 1992. Sophisticated formulas for d in POEM, Boeing Internal Document, October.

Spalart, P.R., Allmaras, S.R., 1994. A one-equation turbulence model for aerodynamic flows. La Rech. Aerospatiale 1, 5–21.

Spalart, P.R., Shur, M., 1997. On the sensitization of turbulence models to rotation and curvature. Aerospace Sci. Technol. 1 (5), 297–302.

Spalding, D.B., 1972. A novel finite difference formulation for differential expressions involving both first and second derivatives. Int. J. Numer. Meth. Eng. 4, 551–561.

Spalding, D.B., 1994. Calculation of turbulent heat transfer in cluttered spaces. In: Presented at the 10th International Heat Transfer Conference, Brighton, UK.

Taneda, S., 1956. Experimental investigation of the wakes behind cylinder and plates at low Reynolds number. J. Phys. Soc., Japan 14, 843–856.

Tucker, P.G., 2003. Differential equation based wall distance computation for DES and RANS. J. Comput. Phys. 190 (1), 229–248, 1st September.

Tucker, P.G., 2001. Computation of Unsteady Internal Flows. Kluwer Academic Publishers, Dordrecht.

Tucker, P.G., Rumsey, C.L., Spalart, P.R., Bartels, R.E., Biedron, R.T., 2005. Computations of wall distances based on differential equations. AIAA J. 43 (3), 539–549.

Tucker, P.G., Pan, Z., 2000. A Cartesian cut cell method for incompressible laminar flow. Appl. Math. Model. 24, 591–606.

Wang, H.P., Goldstein, R.J., Olson, S.J., 1998. Effect of high freestream turbulence with large length scale on blade heat/mass transfer, ASME Paper 98-GT-107.

Wilcox, D.C., 1988. Reassessment of the scale-determining equation for advanced turbulence models. AIAA J. 26 (11), 1299–1310, November.

Wilcox, D.C., 2004. Turbulence Modeling for CFD, second ed. DCW Industries, Inc.

Wolfshtein, K.M., 1969. The velocity and temperature distribution in one-dimensional flow with turbulence augmentation and pressure gradient. Int. J. Heat Mass Transfer 12, 301–318.

Yap, C.R., 1987. Turbulent heat and momentum transfer in recirculating impinging flows. Ph.D. Thesis, Department of Mechanical Engineering, Faculty of Technology, University of Manchester.